IEEE Access
Multidisciplinary | Rapid Review | Open Access Journal

Received August 8, 2020, accepted August 24, 2020, date of publication September 1, 2020, date of current version September 18, 2020.

*Digital Object Identifier 10.1109/ACCESS.2020.3020808*

# Application of Migration Image Registration Algorithm Based on Improved SURF in Remote Sensing Image Mosaic

**TIAN ZHANG[1], RUI ZHAO[2], AND ZHONGSHENG CHEN[3]**

[1]College of Mechanical Engineering, Shenyang Jianzhu University, Shenyang 110168, Liaoning, China
[2]Faculty of Engineering and IT, University of Technology Sydney, Ultimo, NSW 2007, Australia
[3]College of Land and Resources, China West Normal University, Nanchong 637009, China

Corresponding author: Zhongsheng Chen (chenzhs@cwnu.edu.cn)

This work was supported in part by the Natural Science Fund of Liaoning Province under Grant 20180551000, and in part by the Meritocracy Research Funds of China West Normal University under Grant 17YC103.

**ABSTRACT** The classical SURF algorithm has many disadvantages, such as high dimension of feature descriptor, large amount of computation, and low matching accuracy when the angle of rotation and angle of view is too large. To solve the above problems, an improved algorithm is proposed. Firstly, image preprocessing is carried out by image binarization, feature points are extracted by Hes-sian matrix, and then feature description is carried out by using circular neighborhood of feature points. Har wavelet response is used to establish descriptors for each feature point, and the normalized gray-level difference and second-order gradient in the neighborhood are calculated simultaneously to form a new feature descriptor. Finally, the RANSAC algorithm is used to eliminate the mismatch points. The algorithm does not Compared with the classical SURF algorithm, it has the advantage of speed, and makes full use of the gray level information and the detail information, so it has higher accuracy. Experimental results show that the algorithm has good robustness and stability to image blur, illumination difference, angle rotation, field of view transformation and so on. The algorithm is applied to remote sensing image stitching to obtain the stitched image with no obvious geometric shift and good edge connection. This algorithm is a kind of image registration algorithm with short time and high precision, which can meet the registration requirements of remote sensing image stitching.

**INDEX TERMS** Carbon dioxide, image mosaicking, remote sensing image, SURF, RANSAC.

## I. INTRODUCTION

According to the difference of registration methods, image mosaic can be divided into the following three kinds.

Image mosaic algorithm based on gray area is developed from the field of image matching [1]. First, the reference image is segmented into a fixed geometric area, and then the regions of the same size are selected from the image to be stitched, and the similarity of the regions is calculated by using the topological characteristics of the two image regions [2]. In 1982, Rofenfied first proposed the cross-correlation similarity measure to calculate the similarity between regions. Then Barnea proposed Sequential Similarity Detection (SSDA) algorithm [3]. The latter improves the region search strategy of image matching and greatly speeds up the speed of image registration. Then, the geometric region correlation method is proposed. Zhang *et al.* [4]. Apply it to log polar coordinates, and use the non-uniform transformation of log polar coordinates to improve the efficiency of [5]. Chen *et al.* [6] carry on the wavelet transformation to the image, extracts the initial match point set in the low frequency picture, calculates the image similarity on the original picture, thus obtains the matching characteristic spot accurate location [7]. Although the algorithm has high computational efficiency, the matching rate of feature points depends heavily on the feature information of low frequency images, so the correct matching rate is not high.

In 1975, the phase correlation method was proposed by Kuglin. Fourier transform was used to transform the image to time-frequency and calculate the translation vectors of the

The associate editor coordinating the review of this manuscript and approving it for publication was Zhihan Lv.

two images. This method can adapt to the image with great brightness and fast execution speed. In 1987, Xuanyu and Chen [8] improved the phase correlation method by using the Fourier transform property, and realized the fast registration of rotating and changing images. With the rise of the fast Fourier transform, the registration of scaling and changing images is solved by the combination of polar transform and power spectrum. However, the limitation of this method is that it only has better registration effect for images with larger coincidence regions. In 1996, Reddy [9] improved the phase correlation algorithm, making it suitable for image registration with rotation or translation. However, this algorithm can only adapt to rigid change of image registration, and it is not effective for image registration with shape change. Therefore, the phase correlation method of 3D images has become popular. The 3D image registration algorithm mainly uses hierarchical strategy to solve the rigid image transformation model and the non rigid image transformation model respectively [10]. In China, many scholars have studied this algorithm. Li Zhongke combines Hof transform and phase correlation algorithm, and makes full use of fast computation of Fourier transform to quickly rotate and transform images. Guo Yongcai and others used the improved polar coordinate method to obtain image transformation parameters, which improved the registration accuracy of rotating translation images. Phase correlation algorithm is very effective for image translation or rotation transformation. However, when the viewing angle is changed greatly and the image transformation is complex, the algorithm does not give the appropriate solution.

The main idea of feature based image mosaic algorithm is to extract the stable feature points by feature extraction method, to match the feature points, and then transform the image to the same coordinate system according to the image transformation model, so as to achieve the purpose of registration [11], [12]. The key point of the algorithm is how to extract stable feature information from complex scenes and ensure the accuracy and stability of the algorithm. Moravec operator was proposed by Moravec in 1977, which extracts stable feature information based on gray variance and non-maximum suppression of image. In 1988, Harris added the theory of signal to the basis of Moravec operator, and proposed a feature extraction operator based on signal, Harris operator [13]. The algorithm uses the first order difference method to calculate the grayscale change of the image, and the pixels with large gray scale gradient are labeled as feature points. The scale invariant feature transform (SIFT) algorithm proposed by Lowe in 2004 is a very stable algorithm. First, the concept of scale invariant space is proposed, and the extremum points are extracted in the scale space. The position, scale and direction of the stable extremum point are obtained. The algorithm can keep the invariance of feature points under the influence of complex image geometric transformation and noise illumination [14]. However, the matching feature points obtained by the algorithm have some errors, and the accuracy of the algorithm has decreased. The strong stability of SIFT algorithm has attracted the attention of scholars at home and abroad, and the improvement of SIFT algorithm is endless. In 2006, Bay proposed the Speeded Up Robust Feature (SURF) detection algorithm [15]. The algorithm extracted feature points by integral calculation and box filtering, although it accelerated the speed of feature extraction, but the stability of feature points was not as stable as SIFT algorithm. In 2011, Chen [16] Were improved on the basis of SIFT algorithm. The Canny edge feature matching was added to effectively achieve the matching of edge feature points. In 2012, Chen Mengting and others extracted Harris corners and used SIFT algorithm to describe corners. This algorithm overcomes the shortcomings of SIFT algorithm, which takes a long time. Through the comparison of the above three image stitching algorithms, we can see that the feature-based image mosaic algorithm has obvious advantages and practicability. The algorithm is not required for images, and can adapt to complex and varied images such as rotation, translation and zooming. Therefore, the carbon dioxide image mosaic in this paper is based on image registration algorithm based on SIFT features [17]–[19].

Panorama is one of the main methods to immerse virtual reality [20]. Therefore, panoramic image generation technology has gradually become one of the research hotspots in the field of virtual reality in recent years. The traditional panoramic image generation is generally based on 3D graphics modeling and rendering methods, and the panoramic image generation technology based on image rendering (IBR) directly uses the camera to capture the different sequence of images in the same scene, and generates the scene panoramic image based on image mosaic technology. It overcomes the traditional 3D graphics method. The disadvantage reduces the complexity of modeling and rendering [21]. YANG Zhen-hao studied cylindrical projection transformation and image fusion algorithms in panoramic mosaic technology. Through image acquisition, image preprocessing and distortion correction, cylindrical projection transformation, image matching, image mosaic and fusion, a series of steps are completed to transform the image.

Due to the obvious stitching of traditional image stitching, Shuai Wen-Shuang *et al.* [22] have proposed a new method to solve this problem and make the stitching result more smoother. This method is based on SIFT algorithm and morphological component analysis (MCA) in training dictionary [23]. The two core of image mosaic are image registration and fusion. Firstly, SIFT algorithm is used to extract feature points and realize image registration. Then, the K-SVD algorithm is used to train the over complete dictionary based on the original image, and the MCA algorithm is used to decompose the image, so that the decomposed component cartoon and texture are used for image fusion respectively. This method not only guarantees the stitching effect, but also filters the noise contained in the original image [24].

Aiming at the inadequacy of the existing SIFT algorithm in the application of image mosaic technology, Liang *et al.* [25]

proposed an improved block H-SIFT algorithm, which combined with Harris algorithm to block the image before image matching, thus improving the efficiency of image mosaic. Three dimensional accuracy of image matching: Based on weighted smoothing algorithm, the best stitching line is found by using gradient and divergence values of image feature points to achieve seamless image stitching.

In agricultural production, image mosaic plays an important role in panoramic view when real-time sensors are used to collect images [26]–[29]. Because most agricultural operations are carried out externally, the traditional image mosaic method based on SIFT algorithm is affected by uneven illumination and wind [30]. Therefore, there is information dislocation or missing in the mosaic image. It is difficult to meet the reliability requirement of agricultural vehicle application by using image feature elements for image mosaic. To solve this problem, Zhang *et al.* [31] proposed a new image mosaic method based on Kinect color and depth dual information feature source. Firstly, Kinect sensor is used to collect depth information and color image from three different angles. The Kinect sensor is fixed on the slider. When the moving slider moves at a constant speed of 0.5m/s, the Kinect moves at the same speed. The color image and depth information are acquired by calling Kinect in MATLAB and saved every 0.6s. Three consecutive time points are selected and three color images from three angles are selected as mosaic images. Secondly, the SIFT algorithm is used to extract feature points from color images. SIFT algorithm can extract the invariant features of illumination, affine and projection transformation. It helps to reduce the number of feature points matching and improve the speed and accuracy of feature points matching. Thirdly, feature points are matched by similarity measure, and Euclidean distance is used as similarity measure of two images. Get the key points in the image, and find the two closest key points in another image. If the ratio of the nearest distance to the next nearest distance is less than a threshold, the matching points are received [32]. But there are some mismatches in this method. Excessive mismatching may lead to inlaying errors. Therefore, a method of eliminating mismatch is needed to improve the matching accuracy [33]. According to the nature of Kinect, if Kinect moves horizontally, the depth data of fixed points are the same. Based on this feature, some mismatches will be eliminated. If the depth data of the two feature points are the same, the matches are retained, otherwise they will be deleted. As a result, the accuracy of the matching is improved. Secondly, the projection transformation matrix is obtained by RANSAC (Random Sample Consistency) algorithm. The RANSAC algorithm uses the minimum possible point to estimate the model, and then enlarges the influence range of the model as much as possible. Projection transformation matrix is more accurate than traditional image mosaic method because of eliminating mismatch [34]. Finally, the image fusion is relatively smooth through the best suture algorithm. Indoor and outdoor experiments show that the mosaic method based on color and depth dual information feature has obvious advantages, which can effectively overcome the influence of light and wind and other environmental factors, and avoid image splicing errors such as image loss and brightness difference very good [35]–[37]. In indoor experiments, the mosaic method used in this paper is 9.70s. The matching accuracy is 92.9%, while the traditional matching algorithm based on SIFT algorithm is 13.04s, and the matching accuracy is 88.1%. In outdoor testing, the mosaic method used in this paper accounts for 71.15s. The matching accuracy is 99.1%, while the traditional method based on SIFT takes up 77.67s, and the matching accuracy is 92.1%. Therefore, the mosaic method in this paper takes less time than the traditional method based on SIFT algorithm. The test data of stitching accuracy show that the average matching accuracy of the proposed method is 96%, which is 5.9% higher than that of the traditional image mosaic method based on SIFT. Therefore, this method can be further applied to other image mosaic occasions. Accurate spraying and control of drug fertilizer.

From the perspective of overall technology development, image mosaic technology has become more and more mature and stable, and many excellent image stitching algorithms have emerged. However, image mosaic involves a lot of research fields. There are many problems in traditional stitching methods when dealing with special scenes. The global transformation model between the two images obtained by traditional stitching algorithm is very difficult. It is only suitable for long-range shooting and rotating shooting, requiring two images to be in the same plane, and when the image angle changes, the registration error increases significantly. Therefore, this paper deeply studies the key technology and theory of each link of carbon dioxide image mosaic, and finally uses RANSAC algorithm to eliminate mismatched points. This algorithm not only has the advantage of speed over the classical SURF algorithm, but also makes full use of the gray information and detail information, and has higher accuracy.

## II. PROPOSED METHOD

### A. IMAGE PREPROCESSING

The Otsu method is a global dynamic two valued method, also called the Otsu method. It is also called the maximum inter class difference. It is based on the statistics of the whole image and realizes the automatic selection of thresholds. No matter whether the histogram of the image has obvious Shuangfeng, it can get satisfactory results and has been applied and developed in many fields.

For image Image, it is divided into target and background segmentation threshold [38]. The number of target pixels is proportional to the image, and the average gray level is. The total average gray level of the image is: Traversing from the minimum gray value to the maximum gray value is the best threshold for segmentation when the maximum value is made. The Otsu method can be understood as follows: this formula is actually the variance between classes, and the two parts of the target segmentation and the background segmentation constitute the whole image, and the target value, probability,

background value, probability and total mean are obtained according to the definition of variance. Because variance is a measure of the uniformity of the grayscale distribution, the larger the variance is, the greater the difference between the two parts of the image. When some target points are mistaken for the background or some of the background points are divided into target points, the two part difference will be smaller.

It is recorded as the gray value of the image point, and the gray level is, so it is possible to assume the value. The frequency of the gray value is k, there are:

$$p(k) = \frac{1}{MN} \sum_{f(i,j)=k} 1 \tag{1}$$

Assuming that the target and background segmented by the gray value t as the threshold are respectively: sum, then the proportion of the target part is [39]:

$$\omega_0(t) = \sum_{0\le i\le t} p(i) \tag{2}$$

$$\text{Target Partial Points: } N_0(t) = MN \sum_{0\le i\le t} p(i) \tag{3}$$

$$\text{Background portion ratio: } \omega_1(t) = \sum_{t<i\le m-1} p(i) \tag{4}$$

$$\text{Background part points: } N_1(t) = MN \sum_{t<i\le m-1} P(i) \tag{5}$$

$$\text{Target mean: } \mu_0(t) = \sum_{0\le i\le t} ip(i)/\omega_0(t) \tag{6}$$

$$\text{Background mean: } \mu_1(t) = \sum_{t<i\le m-1} ip(i)/\omega_1(t) \tag{7}$$

$$\text{The total mean: } \mu = \omega_0(t)\mu_0(t) + \omega_1(t)\mu_1(t) \tag{8}$$

Otsu method points out that the formula for calculating the optimal threshold g of an image is as follows [40]:

$$g = Arg \underset{0\le t\le m-1}{Max} [\omega_0(t)(\mu_0(t)-\mu)^2 + \omega_1(t)(\mu_1(t)-\mu)^2] \tag{9}$$

The bracket in the right bracket is actually the variance between the classes. The two parts of the target g and the background are composed of the whole image, and the target value $\mu_0(t)$, probability $\omega_1(t)$, background value $\mu_1(t)$, probability $\omega_0(t)$ and total $\mu$ mean are obtained according to the definition of variance. Because variance is a measure of the uniformity of the grayscale distribution, the greater the variance, the greater the difference between the two parts of the image. When the partial target is mistaken for the background or the part of the background error is divided into a target, the difference between the two parts will be smaller. The real meaning. In fact, another way of thinking can also be a good understanding of Otsu method. $\mu_0(t)$ and $\mu_1(t)$, it can represent the center grayscale of the target and the background respectively [41], representing the central gray level of the whole image, and to get the best segmentation of the target and the background. Of course, we want to separate the object as far away from the image center as possible,is to say $(\mu_0(t) - \mu)^2$, or $|\mu_0(t) - \mu|$ as far as possible, and keep the background as far away from the center as possible. so:

(1) the weight and maximum of both:

$$g = Arg \underset{0\le t\le m-1}{Max} [\omega_0(t)(\mu_0(t)-\mu)^2 + \omega_1(t)(\mu_1(t)-\mu)^2] \tag{10}$$

(2) the product of the two is the largest.

$$g = Arg \underset{0\le t\le m-1}{Max} [(\mu_0(t) - \mu)^2(\mu_1(t) - \mu)^2] \tag{11}$$

Notice that there is, and so there $\mu = \omega_0(t)\mu_0(t) + \omega_1(t)\mu_1(t)$, $\mu_0(t) \le \mu \le \mu_1(t)$ is:

$$\omega_0(t)\,(\mu_0(t) - \mu)^2 + \omega_1(t)\,(\mu_1(t) - \mu)^2 = (\mu_0(t) - \mu)^2\,(\mu_1(t) - \mu)^2 \tag{12}$$

### B. IMAGE TRANSFORMATION

Assuming that the gray range of the original image f (x, y) is [a, b], the gray range of the transformed image g (x, y) is linearly extended to [c, d], then the gray value of any point in the image is P (x, y), and the transformation is followed by the following expression [43].

$$g(x, y) = \frac{d-c}{b-a} \times [f(x, y) - a] + c \tag{13}$$

If the gray level distribution of most pixels in the image is in the interval [a and b], Max f is the largest gray level of the original image, and only a small part of the gray level exceeds this interval.

$$g(x, y) = \begin{cases} c & o \le f(x, y) \le a \\ \dfrac{d-c}{b-a} \times [f(x, y) - a] + c & a \le f(x, y) \le b \\ d, & b \le f(x, y) \le \max f \end{cases} \tag{14}$$

Under the condition of under exposure or over exposure, the grayscale of the image may be confined to a very small range, and the resulting image may be a blurred and seemingly ungrayscale image. Linear transformation is used to stretch the gray level of each pixel in the image, which will effectively improve the visual effect of the image.

### C. BASED ON SURF ALGORITHM OF FEATURE EXTRACTION AND MATCHING

The overall thought process of SURF method is similar to SIFT, but different from SIFT is adopted in the whole process. The detection of feature points is still based on the theory of love you in scale space. In image 1, the point at = (x, y) is defined as a Hessian matrix on scale:

$$H = \begin{bmatrix} L_{xx}(\hat{x}, \sigma) & L_{xy}(\hat{x}, \sigma) \\ L_{xy}(\hat{x}, \sigma) & L_{yy}(\hat{x}, \sigma) \end{bmatrix} \tag{15}$$

The second derivative of Gauss filtering is the result of convolution of I = (x, y), in which the Gauss filtering function is $g(\sigma) = \frac{1}{2\pi\sigma^2} e^{-\frac{(x^2+y^2)}{2\sigma^2}}$, and $L_{xy}, L_{yy}$ is the meaning is similar.

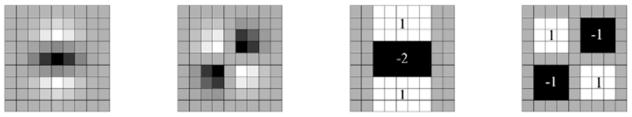


**FIGURE 1.** Scale space generation.

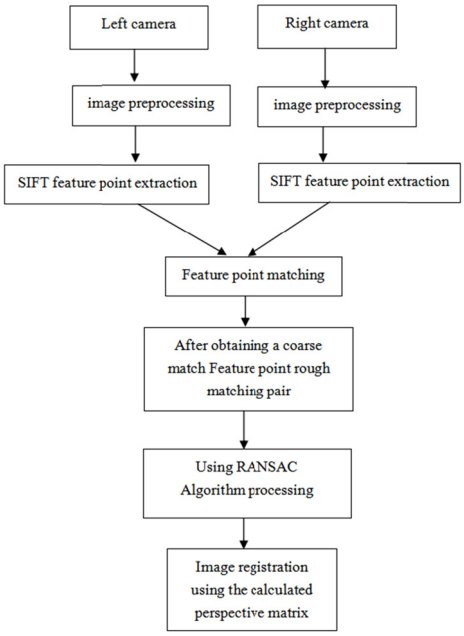


**FIGURE 2.** Flow of image stitching algorithm.

Bay *et al.* proposed to replace the second-order Gauss filter with the square filter approximation and accelerate the convolution with the integral image to improve the computational speed. In the original image, the image of Pyramid with different scales is formed by enlarging the size of the box. The frame filter template value of 9*9 is shown in Figure 1, the gray part template value is 0, corresponding to the two order Gauss filter = 1.2 and the corresponding scale value s == 1.2, and the value of the square filter template is convoluted with the image, respectively, $D_{xx}$, $D_{xy}$, and the $D_{yy}$. He is further solved the expression of the ssian matrix:

$$\Delta(H) = D_{xx}D_{yy} - (0.9D_{xy})^2 \tag{16}$$

Scale image pyramids are constructed using SIFT-like methods. Four-level scale images are selected in each order, and the construction parameters of the fourth order are shown in Figure 2. The number on the grey bottom indicates the size of the filter template. If the size of the image is much larger than that of the template, the order can be increased. If the filter template size is N*N, the corresponding scale s = 1.2*N/9; using Hessian moments.

Taking the feature point as the center, the coordinate axis is first rotated to the main direction, and the square area with a length of 20s is selected according to the main direction. The window area is divided into sub regions of 4*4. In each sub region, the wavelet response in the range of 5s*5s (sampling step size s) is calculated, which is relative to the horizontal and vertical Haar in the main direction. The wavelet responses are recorded as DX and Dy respectively, giving the response value a weight coefficient to increase the robustness to the geometric transformation. In this way, vectors of four-dimensional components are formed in each sub-region.

$$V_{sub} = (\sum d_x, \sum |d_x|, \sum d_y, \sum |d_y|) \tag{17}$$

Therefore, for each feature point, a 4*4*4 = 64-dimensional description vector is formed, and then the vector is normalized, which is robust to illumination.

### D. ELIMINATION OF MISMATCH POINTS BY RANSAC ALGORITHM

RANSAC algorithm can be said to be a mathematical model of iterative algorithm. His main principle is to find some feature points, and then according to these characteristics, a straight line is formed. In this line, the points in this line are counted in a certain error range, then repeat this step, and finally select the points with the largest number of points. As the final result. This idea is also the reason why he is often used in image matching. From the experience of predecessors, we can get the matrix form of RANSAC algorithm:

$$\begin{bmatrix} x' \\ y' \\ 1 \end{bmatrix} = \begin{bmatrix} h1 & h2 & h3 \\ h4 & h5 & h6 \\ h7 & h8 & h9 \end{bmatrix} \begin{bmatrix} x \\ y \\ 1 \end{bmatrix} \tag{18}$$

In determining a straight line, according to mathematical knowledge, we need two points. Here we have to find two matching points. If we determine the 9 parameters of the above matrix, we need 8 matching points.

In this algorithm, another key parameter is the setting of the threshold. In order to solve this threshold, we should introduce several concepts and functions. First, we assume that the error is in line with the Gauss distribution, and the distance error square satisfies the x square distribution of M. So you can get the following function formula:

$$Fm(k^2) = \int_0^{k^2} Xm^2(\xi)d\xi < k^2 \tag{19}$$

From the above, we get the method of calculating the threshold.

$$t^2 = Fm^{-1}(\alpha)\sigma^2 \tag{20}$$

Mathematical function expression is a priori probability, so when calculating the threshold, it is the first step to calculate, and then the threshold can be determined according to the above formula. After the threshold is determined, the next step is to judge the internal points, which can be based on the following functions:

$$s = \left\| H * \mathrm{i} - i' \right\|^2 \tag{21}$$

In the above function expression, I represents the coordinates of the matching points obtained by multiplying with

the matrix. The coordinates are chosen from the selected matching points to get the error s. According to the size of the error and the size of the threshold, the feature points are judged. If it is less than the threshold, it is the internal point, otherwise it is not.

In the above algorithm, the various methods of matching are clearly defined, but this method has some limitations in practice. First of all, it can not handle large amount of data, because in a relatively high complexity, when calculating the matrix H, it will be calculated one by one, and the efficiency will be reduced, and the time will be increased accidentally. The degree of complexity. So in practical application, we can do this. In the initial matching point, we use 8 points to determine the matrix H, select 4 additional points for judgement, judge when the matrix is determined, if not the internal point is directly abandoned, this will greatly reduce the computation time. The application of this method in high-definition images with high quality and large amount of information requires more matching points, but the time saved increases.

## III. EXPERIMENTS

### A. SURF FEATURE POINT EXTRACTION AND MATCHING MODEL

The SURF algorithm based on SIFT algorithm has the characteristics of scale invariance, rotation invariance and partial perspective invariance. Compared with similar algorithms, the algorithm has good robustness and has obvious real-time advantage in computation. The detailed implementation steps of the SURF algorithm are as follows:

1) to establish an integral image
2) construction of scale space
3) determination of extreme points in scale space
4) determine the key point direction
5) generation of key point descriptors

1. The integral image SURF algorithm is established to satisfy the invariable characteristics of rotation and translation. The filtering process of Gauss's two order differential template in SIFT algorithm is simplified and transformed into the arithmetic operation between integral images. Thus, the algorithm has the advantage of less computation and faster speed than other similar algorithms. The application of the integral image is one of the main reasons for the speed-up of the algorithm. By calculating the sum of the pixel values of any point (x, y) in the original image and all points in the rectangular region formed by the upper left corner of the image, the integral image can be obtained.

When calculating the gray level of the pixels in the window, the size of the window can be ignored. We only need to pay attention to the integral image values of four points in the window: 1, 2, 3 and 4, and calculate them through four corresponding values. The integral image of point 4 in the graph is the accumulation of all the pixel gray values in the D region; similarly, 3 integral points are the sum of the D and C regions; 1 points are the sum of the A and D regions; the 2 integral points are the sum of the gray values of the four regions of A, B, C and D. If only the gray value of B region needs to be calculated, it can be obtained through the point 2, the integral image minus point 3, the minus point 1 and the plus point 4. If there is an image with a gray value of 1, then the integral value at any pixel in the image is equal to the area of the rectangle. The rectangle is determined by the point from the upper left corner of the original image. Figure 1 shows the flow of image stitching algorithm.

From the calculation process, it can be seen that the sum of the gray values of a certain area can be obtained by look-up table and simple arithmetic operations. The complexity of the computation process will not be affected by the size change of the rectangular area of the image, that is, the pixel gray level in the window is not related to the size of the window, which makes the calculation process simple and computable. The speed is obviously accelerated.

### B. IMPROVEMENT OF STITCHING ALGORITHM

In the previous section of this chapter, the key steps of the algorithm are introduced in detail from the algorithm itself. Because the image of rock casting slice itself has the characteristics of complex microstructure, large similarity and particle yelling, and so on, even smaller images may produce more feature points. In the process of image registration, too many feature points will undoubtedly increase the amount of computation, produce time redundancy, and have a fatal impact on stitching speed. At the same time, too many feature points will also increase the number of false matching points [42]. The traditional SURF algorithm has the following main problems in image mosaic of rock casting sheet:

First, the SURF algorithm is oriented to the range of the whole image in the detection of feature points. In practical applications, registration is only the feature points of the overlapped parts in the image. The feature points detected by the non overlapping part are not only meaningless in matching, but also affect the matching accuracy. The amount of operation is greatly increased.

(1) The influence of matching accuracy is reflected in: when there are feature points pairs in non-overlapping areas of mosaic image in matching point pairs, it must be the wrong matching point pairs. Determining the transformation matrix between two images is the main task of image stitching according to the feature points, and the meaningful feature set can only be composed of points extracted from overlapping regions, so the points extracted from non overlapping regions should be eliminated, so as to avoid affecting the accuracy of the transformed matrix.

(2) the increase of computation is reflected in the feature matching stage. When searching for matching points for a specific feature point, the SURF algorithm traverses all the detected feature points one by one. The number of iterations increases with the number of feature points. If the number of iterations is too large, the number of similarity computation will increase correspondingly. Add, will undoubtedly bring a lot of time redundancy.

Secondly, the traditional SURF algorithm uses Euclidean distance to calculate the similarity of feature vectors between

**TABLE 1.** Experimental time comparison (unit: second).

| Group number | Experimental method | 1 | 2 | 3 | 4 | 5 | 6 | 7 | 8 | Average |
|---|---|---|---|---|---|---|---|---|---|---|
| 1 | Original algorithm | 9.17 | 9.35 | 9.47 | 9.12 | 9.51 | 9.27 | 9.96 | 9.48 | 8.48 |
| | Improved algorithm | 9.07 | 9.12 | 9.31 | 9.05 | 9.13 | 9.17 | 9.15 | 9.30 | 9.16 |
| 2 | Original algorithm | 9.89 | 9.67 | 9.15 | 9.57 | 9.68 | 9.56 | 9.17 | 9.64 | 8.70 |
| | Improved algorithm | 9.02 | 9.41 | 9.05 | 9.27 | 9.51 | 9.44 | 9.03 | 9.15 | 9.24 |
| 3 | Original algorithm | 9.15 | 9.59 | 9.62 | 9.57 | 9.73 | 9.71 | 9.65 | 9.86 | 8.88 |
| | Improved algorithm | 8.94 | 9.05 | 9.17 | 9.31 | 9.45 | 9.58 | 9.16 | 9.62 | 9.29 |
| 4 | Original algorithm | 9.64 | 9.15 | 9.68 | 9.63 | 9.78 | 9.56 | 9.84 | 9.16 | 8.94 |
| | Improved algorithm | 8.16 | 9.02 | 9.15 | 9.31 | 9.47 | 9.21 | 9.61 | 9.05 | 9.12 |
| 5 | Original algorithm | 9.89 | 9.15 | 9.84 | 9.45 | 9.56 | 9.45 | 9.76 | 9.48 | 9.06 |
| | Improved algorithm | 9.19 | 9.13 | 9.68 | 9.41 | 9.42 | 9.32 | 9.15 | 9.13 | 9.30 |
| 6 | Original algorithm | 9.56 | 9.47 | 9.19 | 9.88 | 9.47 | 9.98 | 9.14 | 9.08 | 9.09 |
| | Improved algorithm | 9.32 | 9.35 | 9.11 | 9.74 | 9.45 | 9.65 | 9.05 | 9.03 | 9.34 |
| 7 | Original algorithm | 9.15 | 9.28 | 9.56 | 9.47 | 9.65 | 9.48 | 9.96 | 9.16 | 9.19 |
| | Improved algorithm | 9.12 | 9.16 | 9.32 | 9.12 | 9.14 | 9.26 | 9.57 | 9.02 | 9.21 |
| 8 | Original algorithm | 9.78 | 9.46 | 9.26 | 9.17 | 9.19 | 9.48 | 9.56 | 9.87 | 9.31 |
| | Improved algorithm | 9.45 | 9.26 | 9.15 | 9.06 | 9.08 | 9.37 | 9.45 | 9.67 | 9.31 |
| 9 | Original algorithm | 9.45 | 9.56 | 9.52 | 9.48 | 9.78 | 9.86 | 9.15 | 9.69 | 9.50 |
| | Improved algorithm | 9.33 | 9.45 | 9.42 | 9.37 | 9.65 | 9.48 | 9.45 | 9.16 | 9.41 |
| 10 | Original algorithm | 9.36 | 9.45 | 9.18 | 9.56 | 9.89 | 9.84 | 9.56 | 9.78 | 9.62 |
| | Improved algorithm | 9.26 | 9.32 | 9.07 | 9.46 | 9.49 | 9.58 | 9.17 | 9.51 | 9.36 |

two images. From the foregoing, we can see that the algorithm produces a feature vector of dimension 64. When the dimension increases, the Euclidean distance will show insensitivity, which will greatly weaken the matching effect and increase the false matching rate.

Third, most of the time, the one-way matching between the reference image and the target image will be selected. Although this method can save some time, it can not avoid the one to many matching problem in the image with higher similarity.

## IV. DISCUSSION

### A. ALGORITHM EFFICIENCY

In this paper, ten groups of rock image data are used to simulate the algorithm, and each group of data is subjected to 8 experiments, and the data of the algorithm running time are quantified and compared by Table 1.

The running time of the 80 sets of simulation is statistically analyzed. It is found that the median running time of the algorithm is 9.125s before the algorithm is improved, and the median running time of the improved algorithm is 8.49s. The total running time of the improved algorithm is 779.91s, and the total running time of the improved algorithm is 666.51s; the average running time of the improved algorithm is 9.75s, and the improved algorithm runs on average. The time is 8.33s, the standard deviation of running time of the improved algorithm is 2.02, and the standard deviation of running time of the improved algorithm is 1.05. Through calculation, it is found that compared with the improved algorithm, the efficiency of the improved algorithm is increased by about 17%, and the stitching speed of the improved algorithm is obviously faster, which verifies the validity of the algorithm in this paper.

### B. ALGORITHM STABILITY

The running time of Table 1 is averaged, and the ten sets of experimental running time statistics are drawn into columnar charts. The running time of the improved algorithm and the improved algorithm is analyzed more intuitively, and the running time polygon diagram is shown in Figure 2.

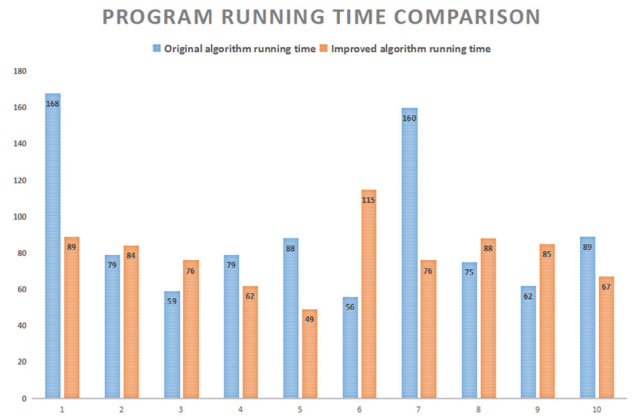


**FIGURE 3.** Comparison of program running time.

Compared with the broken line graph, we can see that due to the influence of image quality, the feature points that may be extracted suddenly increase, and the running time of the algorithm is uneven before the algorithm is improved. The running time of the algorithm is even 2-3 times that of the improved algorithm, and the running time of the improved algorithm is basically kept in a dynamic range. The improved algorithm has better time stability.

### C. ALGORITHM ACCURACY

The improved algorithm is based on the operation of the whole image, that is, the transformation relationship between the images is also determined in the global scope, so that the transformation relationship may be affected by the non overlapping area of the image, and the transformation obtained when the non overlapping area of the two images is distorted or distorted. The accuracy of the matrix will be affected. It may result in the phenomenon of edge vacancy in the image after the completion of the stitching, and enlarge the edge of the image.

80 sets of experiments were carried out on the original algorithm. After statistics, it was found that there were 67 groups in the result of stitching, and the other 13 groups did not show obvious vacancy phenomenon. The correct rate of stitching was 83.75%. The same 80 groups of images were used, and the improved algorithm was used to splice. In the 80 groups of mosaic images, the edges of mosaic results are more regular, and there is no edge vacancy. The correct rate of mosaic is 100%.

## V. CONCLUSION

The early image mosaic algorithm is usually based on the following two premises: first, the camera only performs pure rotation; two, the scene is a plane scene or can be approximated to a plane scene. However, this premise assumes that the hardware requirements are high, and the parallax tolerance of image mosaic algorithm is poor under general circumstances. Recently, parallax image mosaic algorithms have been widely studied, but the quality of image stitching is uneven. There are still various problems in the classic image stitching algorithm.

Even though the image mosaic algorithm has been deeply studied in this paper, most of the problems have been solved. However, there are also some shortcomings in the research process, as well as several problems that are difficult to solve. In this paper, the shortcomings and problems are elaborated in order to optimize and improve the follow-up study. For example, feature extraction. In this paper, we find that in different scenarios, we usually get different number of special refreshing points. This is because the texture features in the scene are not uniform and should be a normal phenomenon. However, the number of features is too small in the past, which will cause the subsequent images to be uneven, while the number of features is too large, which will cause time-consuming operation. How to control the number of features in different scenarios is a problem worth studying.

## REFERENCES

[1] S. Wan, Y. Xia, L. Qi, Y.-H. Yang, and M. Atiquzzaman, "Automated colorization of a grayscale image with seed points propagation," *IEEE Trans. Multimedia*, vol. 22, no. 7, pp. 1756–1768, Jul. 2020.
[2] X. Fu, P. Pace, G. Aloi, L. Yang, and G. Fortino, "Topology optimization against cascading failures on wireless sensor networks using a memetic algorithm," *Comput. Netw.*, vol. 177, Aug. 2020, Art. no. 107327.
[3] M. Kumar, Y. Mao, Y. Wang, T. Qiu, Y. Chenggen, and W. Zhang, "Fuzzy theoretic approach to signals and systems: Static systems," *Inf. Sci.*, vols. 418–419, pp. 668–702, Dec. 2017.
[4] W. Zhang, J. Yang, Y. Fang, H. Chen, Y. Mao, and M. Kumar, "Analytical fuzzy approach to biological data analysis," Saudi *J. Biol. Sci.* vol. 24, no. 3, pp. 563–573, 2017.
[5] Z. Yang, "Image mosaic technology based on cylinder transformation," *Mod. Comput.*, vol. 41, no. 10, pp. 11–14, Apr. 2018.
[6] S. Chen, Y. Lu, Q. Gao, D. Sun, Y. Xia, and X. Peng, "Image mosaic based on SIFT and morphological component analysis," in *Proc. 10th Int. Congr. Image Signal Process., Biomed. Eng. Informat. (CISP-BMEI)*, Oct. 2017, pp. 1–6.
[7] H. Zeng and Y. Ma, "UAV aerial image mosaic algorithms based on improved ORB," *Ind. Control Comput.*, vol. 31, no. 5, pp. 90–92, May 2018.
[8] X. Li and R. Chen, "Research on image mosaic technology based on block H-SIFT algorithm," *J. Henan Inst. Sci. Technol.*, vol. 46, no. 2, pp. 48–51, May 2018.
[9] Y. Shen, J. Zhu, H. Liu, and L. Sun, "Plant image mosaic based on depth and color dual information feature source from Kinect," *Trans. Chin. Soc. Agricult. Eng.*, vol. 34, no. 5, pp. 176–182, Mar. 2018.
[10] B. Wang, F. C. Zou, and X. W. Liu, "New algorithm to generate the adversarial example of image," *Optik*, vol. 207, Apr. 2020, Art. no. 164477.
[11] P. Xu, G. Liu, and Y. Zheng, "Research on document image mosaic algorithm for electronic video magnify system," *Comput. Meas. Control*, vol. 26, no. 2, pp. 227–231, Feb. 2018.
[12] F.-B. Wang, P. Tu, C. Wu, L. Chen, and D. Feng, "Multi-image mosaic with SIFT and vision measurement for microscale structures processed by femtosecond laser," *Opt. Lasers Eng.*, vol. 100, pp. 124–130, Jan. 2018.
[13] C.-L. Wei and C.-T. Ho, "Exploring signaling roles of service Providers' reputation and competence in influencing perceptions of service quality and outsourcing intentions," *J. Organizational End User Comput.*, vol. 31, no. 1, pp. 86–109, Jan. 2019.
[14] Y. Zhao and C. Yang, "Information fusion robust guaranteed cost Kalman estimators with uncertain noise variances and missing measurements," *Int. J. Syst. Sci.*, vol. 50, no. 15, pp. 2853–2869, 2019, doi: 10.1080/00207721.2019.1690719.
[15] C. Yang, Z. Yang, and Z. Deng, "Robust weighted state fusion Kalman estimators for networked systems with mixed uncertainties," *Inf. Fusion*, vol. 45, pp. 246–265, Jan. 2019, doi: 10.1016/j.inffus.2018.01.014.
[16] D. Chen, "Model of weighted local entropy feather image mosaic," *Bull. Sci. Technol.*, vol. 34, no. 3, pp. 179–182, Mar. 2018.

[17] Y. Fu, Y. Zheng, H. Huang, I. Sato, and Y. Sato, "Hyperspectral image super-resolution with a mosaic RGB image," *IEEE Trans. Image Process.*, vol. 27, no. 11, pp. 5539–5552, Nov. 2018.

[18] Q. Chen, J. Zhao, W. Peng, Y. She, and L. Liu, "Close-range image feature recognition and seamless mosaic for railway track," *J. China Railway Soc.*, vol. 40, no. 1, pp. 63–68, Jan. 2018.

[19] X. Gao, S. Zhu, and R. Li, "A image mosaic method based on position and attitude information for small UAV images," *Sci. Surveying Mapping*, vol. 43, no. 2, pp. 70–76, Jan. 2018.

[20] Z. Lv, D. Chen, R. Lou, and H. Song, "Industrial security solution for virtual reality," *IEEE Internet Things J.*, early access, Jul. 1, 2020, doi: 10.1109/JIOT.2020.3004469.

[21] X. Chen, H. Liu, M. Zhou, F. Zhang, and Q. Li, "Medical image mosaic based on low-overlapping regions," in *Proc. 10th Int. Congr. Image Signal Process., Biomed. Eng. Informat. (CISP-BMEI)*, Oct. 2017, pp. 1–5.

[22] W. U. Wen-Shuang, F. E. N. G. Hua-Jun, and X. U. Zhi-Hai, "Optical image mosaic methods based on MEMS gyroscope," *Acta Photonica Sinica*, vol. 47, no. 3, 2018, Art. no. 310001.

[23] Z. Gao, H.-Z. Xuan, H. Zhang, S. Wan, and K.-K.-R. Choo, "Adaptive fusion and category-level dictionary learning model for multiview human action recognition," *IEEE Internet Things J.*, vol. 6, no. 6, pp. 9280–9293, Dec. 2019.

[24] B. Wang, L. L. Chen, and M. Wang, "Novel image segmentation method based on PCNN," *Optik*, vol. 187, pp. 193–197, Jun. 2019.

[25] N. Liang, B. Jia, M. Zhang, Y. Wang, and B. Wu, "Multi-view image mosaic algorithm based on improved scale invariant feature transform in operation room application," *Beijing, China Biomed. Eng.*, vol. 33, no. 1, pp. 9–14, Jan. 2018.

[26] P. Wang, G. Turcatel, C. Arnesano, D. Warburton, S. E. Fraser, and F. Cutrale, "Fiber pattern removal and image reconstruction method for snapshot mosaic hyperspectral endoscopic images," *Biomed. Opt. Express*, vol. 9, no. 2, p. 780, Feb. 2018.

[27] C. Sun, X. Huifang, and Y. Qiao, "Processing of color consistency on orthovista for mosaic of multi-source and multi-temporal satellite image," *Geomatics Spatial Inf. Technol.*, vol. 41, no. 5, pp. 115–117, May 2018.

[28] K. Shinoda, M. Hasegawa, M. Yamaguchi, and A. Ortega, "Mosaicked multispectral image compression based on inter- and intra-band correlation," 2018, *arXiv:1801.03577*. [Online]. Available: https://arxiv.org/abs/1801.03577

[29] Z. Libo, H. Tian, G. Chunyun, and M. Elhoseny, "Real-time detection of cole diseases and insect pests in wireless sensor networks," *J. Intell. Fuzzy Syst.*, vol. 37, no. 16, pp. 1–12, 2019.

[30] I. Kitouni, D. Benmerzoug, and F. Lezzar, "Smart agricultural enterprise system based on integration of Internet of Things and agent technology," *J. Organizational End User Comput.*, vol. 30, no. 4, pp. 64–82, Oct. 2018.

[31] J. Zhang, H. Zhai, L. Huang, and Q. Yu, "Parallax image stitching algorithm based on feature blocking," *Comput. Eng.*, vol. 44, no. 5, pp. 220–226, May 2018.

[32] J. Ren, N. Wang, Z. Wang, L. Ren, and H. Lou, "Research on remote sensing image of UAV fusion algorithm," *J. Jilin Univ.*, vol. 36, no. 2, pp. 142–149, Mar. 2018.

[33] E. J. Leonard, R. T. Pappalardo, and A. Yin, "Analysis of very-high-resolution galileo images and implications for resurfacing mechanisms on europa," *Icarus*, vol. 312, pp. 100–120, Sep. 2018.

[34] H.-B. Zeng, X.-G. Liu, and W. Wang, "A generalized free-matrix-based integral inequality for stability analysis of time-varying delay systems," *Appl. Math. Comput.*, vol. 354, pp. 1–8, Aug. 2019.

[35] H. C. de Oliveira, A. P. D. Poz, M. Galo, and A. F. Habib, "Surface gradient approach for occlusion detection based on triangulated irregular network for true orthophoto generation," *IEEE J. Sel. Topics Appl. Earth Observ. Remote Sens.*, vol. 11, no. 2, pp. 443–457, Feb. 2018.

[36] W. Zhu, S. Li, X. Zhang, Y. Li, and Z. Sun, "Estimation of winter wheat yield using optimal vegetation indices from unmanned aerial vehicle remote sensing," *Trans. Chin. Soc. Agricult. Eng.*, vol. 34, no. 11, pp. 78–86, 2018.

[37] L. Tang, W. He, Q. Li, D. Zhang, W. Wang, and X. Hu, "The algorithm for the recognition of pointer type meter based on space transformation," *Elect. Meas. Instrum.*, vol. 55, no. 6, pp. 116–121, Mar. 2018.

[38] Y. Liu, C. Yang, and Q. Sun, "Thresholds based image extraction schemes in big data environment in intelligent traffic management," *IEEE Trans. Intell. Transp. Syst.*, early access, Jun. 5, 2020, doi: 10.1109/TITS.2020.2994386.

[39] S. Zhao, B. Kang, and L. Wang, "The video stabilization algorithm based on MEMS gyroscope," *J. Northwest Univ.*, vol. 48, no. 3, pp. 355–362, Jun. 2018.

[40] F. Yanjun, W. Lingxiao, and Huming, "Research on critical method of large objects three-dimensional measurement based on monocular structured light," *J. Appl. Opt.*, vol. 39, no. 2, pp. 52–57, 2018.

[41] F. Xiong, G. Wang, Y. Chen, X. Li, and Z. Chen, "Research on intelligent measurement system for large size complex fine blanking parts," *Comput. Meas. Control*, vol. 26, no. 1, pp. 55–58, Jan. 2018.

[42] J. Wang, J. Fang, X. Wang, and J. Ma, "Image stitching model of axis-shift multi digital camera and its self-calibration," *Opt. Technique*, vol. 44, no. 1, pp. 94–100, Jan. 2018.

[43] D. Li, L. Xiao, J. Tian, and J. Sun, "Multi-images mosaic algorithm based on improved phase correlation and feature point registration," *Comput. Sci.*, vol. 45, no. 1, pp. 313–319, Jan. 2018.


**TIAN ZHANG** was born in Shenyang, Liaoning, China, in 1985. He received the bachelor's degree from Jiangnan University, China, the master's degree from Northeastern University, China, and the Ph.D. degree from the Beijing Institute of Technology, China. He is currently a Lecturer with the College of Mechanical Engineering, Shenyang Jianzhu University. His research interest includes vision-based measurement and inspection technology, image processing, and registration algorithm.

**RUI ZHAO (AKIRA)** is currently pursuing the Ph.D. degree with the Faculty of Engineering and Information Technology (FEIT), University of Technology Sydney.

She is also a Researcher and a Programmer with the FEIT, University of Technology Sydney. Her research interests are span different disciplines, including algorithm design, human–computer interaction, data visualization design, designing interactive systems, computer vision, cyber security, and artificial intelligence.

**ZHONGSHENG CHEN** was born in Heze, Shandong, China, in 1981. He received the Ph.D. degree in cartography and geographical information system from East China Normal University. He currently works with the College of Land and Resources, China West Normal University. His current research interests include machine learning, computational intelligence, image processing, remote sensing, and geographical information systems.